Monitoring Monopile Penetration Through Magnetic Stray Field Measurements

Meijers, P.C.; Tsouvalas, A.; Metrikine, A.

DOI
10.47964/1120.9102.19534

Publication date
2020

Document Version
Final published version

Published in
EURODYN 2020 XI International Conference on Structural Dynamics

Available online at www.easdprocedia.org
EASD Procedia EURODYN (2020) 1272-1280

EASD Procedia

EURODYN 2020
XI International Conference on Structural Dynamics
M. Papadrakakis, M. Fragiadakis, C. Papadimitriou (eds.)
Athens, Greece, 23–26 November 2020

MONITORING MONOPILE PENETRATION THROUGH MAGNETIC STRAY FIELD MEASUREMENTS

Peter C. Meijers[1], **Apostolos Tsouvalas**[1], **and Andrei V. Metrikine**[1]

[1]Delft University of Technology,
Faculty of Civil Engineering and Geosciences,
Stevinweg 1, 2628 CN
Delft, the Netherlands
e-mail: {p.c.meijers,a.tsouvalas,a.metrikine}@tudelft.nl

Keywords: Pile penetration monitoring, Non-contact method, Magnetic stray field.

Abstract. *Current methods to infer the penetration of a steel monopile during an offshore installation are rather inaccurate. Since a large number of foundation piles will be installed offshore in the coming years, a reliable technique to infer the penetration depth is vital. This paper proposes a non-contact method to monitor the pile progression into the seabed based on measurements of the magnetic stray field that permeates the air surrounding the structure, eliminating the necessity of a predefined pattern on the pile's surface. A simple magnetisation model for the monopile is proposed from which the relative motion between the moving pile and a stationary magnetic field sensor can be extracted. Comparison between the measured and simulated stray field data show a promising correlation, providing the basis for the new non-contact monitoring technique that is applicable offshore.*

ISSN:2311-9020
Peer-review under responsibility of the Organizing Committee of EURODYN 2020.
doi: 10.47964/1120.9102.19534

1 INTRODUCTION

In the coming years, a large number of offshore wind farms will be commissioned in the North Sea. The most popular foundation type for wind turbines is the monopile [1], which is a cylindrical shell structure consisting of multiple steel sheets that are welded together. Currently, nearly all of these piles are gradually driven into the seabed by means of hydraulic impact hammers. Real-time knowledge of the pile penetration resulting from each hammer blow is vital to ensure safety during the installation process and to limit the amount of fatigue damage inflicted to the pile, since the energy of the blows can be adjusted accordingly based on the penetration speed. Moreover, after installation, the bearing capacity of the pile is estimated by measuring the pile's response to a single axial impact in a so-called restrike test [2].

Several techniques currently exist to monitor pile penetration. By registering the acceleration with a sensor mounted to the pile, the penetration is computed by integrating the signal twice in time [3]. Disadvantages of this approach include the need to attach the sensor to the surface of the pile, which is a delicate and time-consuming process, and the error in the computed displacement that accumulates due to filtering choices and the integration of the acceleration signal. Alternative techniques rely on optical signals. One such method is to deduce the distance between the top of the pile and a reference level based on the time-of-flight principle [4]. However, in an offshore environment, a steady reference level is not available, since optical signals, instead of reflecting back to the detector, scatter as result of the surface waves at the water level. A different optical approach is to use a camera to track a predefined pattern that is applied to the surface of the pile, e.g. a black and white banded pattern. Several patterns have successfully been administered over the years, especially in the case of restrike tests [5–8]. These approaches share the necessity to prepare the surface of the pile with a distinct predefined visual pattern.

Ideally, a method to register pile penetration is based on a non-contact sensor, simplifying the deployment significantly. Furthermore, such an optimal method does not require any preparation of the pile's surface to operate, i.e. no pattern has to be introduced. A method based on the magnetic stray field generated by a steel structure in the presence of the geomagnetic field could satisfy both of these criteria, since the stray field permeates the space surrounding the monopile. Hence, this paper investigates the feasibility to use the magnetic stray field to monitor the pile's penetration during installation. To this end, first, stray field data measured during a full-scale onshore monopile installation are presented, examining change of the magnetic signature of the structure with increasing penetration depth. Second, the magnetic stray field of the structure is simulated by employing a simple model for the structure's magnetic susceptibility that includes the presence of circumferential welds. Third, the possibility to utilise stray field measurements to determine the relative motion between the pile and a magnetic field sensor is discussed. Finally, the main conclusions of this work are summarised.

2 FULL-SCALE MEASUREMENT CAMPAIGN

During the installation of a steel monopile, the magnetic stray field has continuously been measured by means of a stationary magnetometer, which is mounted on top of a ground-based tripod. Since this concerns an onshore installation, a suitable reference level is available (ground level), allowing for a time-of-flight laser sensor to be employed to measure the pile's penetration in conjunction with the magnetic stray field measurements.

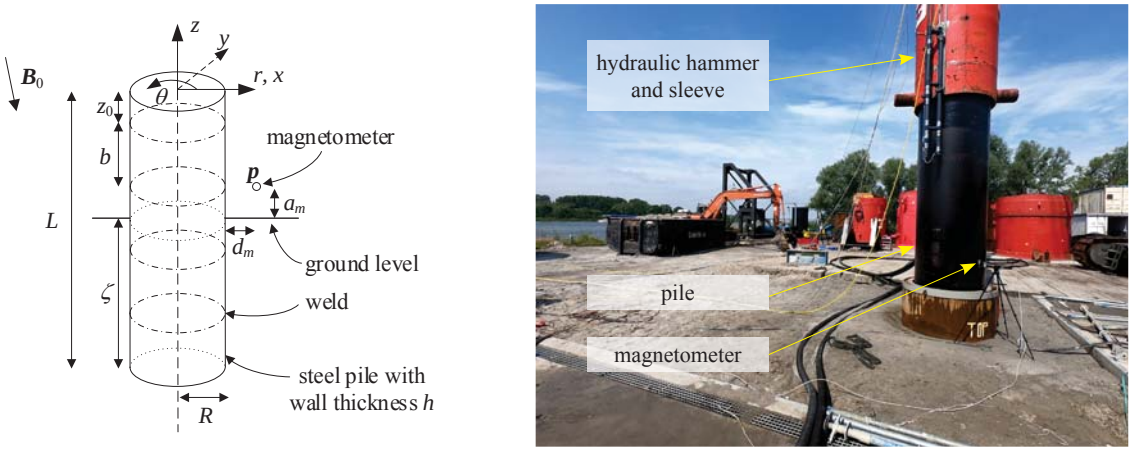

Figure 1: Set-up of the full-scale onshore monopile installation. (a) Schematic indicating the parameters of interest. (b) Photograph of the installation site.

2.1 Description of the set-up

A schematic of the set-up of the pile installation is presented in Figure 1a, which defines two coordinates systems: a cylindrical $r\theta z$-coordinate system—in which r, θ, and z denote the radial, the circumferential, and the axial directions, respectively—and a Cartesian xyz-coordinate system. The coordinate systems share their origin, which is located at the top of the pile. Table 1 lists the numerical values of the relevant parameters of the pile: the radius R, length L, and wall thickness h. The installed pile is composed of cylindrical steel sections with a height b each, which are stacked on top of each other using circumferential welds. Before installation, the pile has been coated for corrosion protection, obscuring the exact locations of the welds. Despite the lack of visible confirmation, their positions relative to the pile top are known *a priori*. The distance z_0 reflects the shorter top segment of pile.

To determine the penetration, a time-of-flight distance sensor is attached to the sleeve of the hydraulic hammer, which is depicted in Figure 1b. The current penetration depth ζ is defined as the distance from lower end of the pile to the ground level, implying that the pile is fully embedded into the soil when $\zeta = L$. The initial penetration depth ζ_0 is also listed in Table 1.

A biaxial magnetometer (type: HMC1022) registers the magnetic stray field while the pile gradually progresses into the soil with each hammer blow. It measures the two dominant components of the stray field: the radial B_r and the axial B_z. Figure 1b shows the magnetometer mounted on top of a tripod. Its position $\boldsymbol{p}$ relative to the ground is given by the offset from the pile's surface d_m, the circumferential position θ_m and the height a_m as specified in Table 1. A final parameter of importance is the direction and intensity of the geomagnetic field, of which the components expressed in the Cartesian xyz-coordinate system are $\boldsymbol{B}_0 = [B_0^x \;\; B_0^y \;\; B_0^z]^T = [15 \;\; 10 \;\; -40]^T\,\mu$T, signalling that it has a predominantly downward component. For the current purpose, the external field is considered to be time and space invariant.

2.2 Magnetic stray field versus penetration depth

Figure 2 shows the magnetic stray field components plotted against the measured penetration depth ζ. Both components of $\boldsymbol{B}$ show a pattern that repeats every 3 m, which is caused by the circumferential welds in the pile. Compared to the fairly homogeneous material in between

Parameter	Value
R	0.6096 m
L	62.0 m
h	0.050 m
b	3.0 m
z_0	0.5 m
ζ_0	48.62 m
a_m	1.5 m
θ_m	300°
d_m	0.2 m

Table 1: Parameters of interest for the pile installed during the measurement campaign.

them, the welds have significantly different magnetic properties, resulting in a local reduction of the magnetic susceptibility, which in turn create distinct markings in the field. Furthermore, it is clear that the magnitude of the radial component B_r increases when the pile penetrates further into the soil, which can be attributed to the sensor approaching the top of the pile. Due to the repeated impacts of the hammer, the pile has become magnetised in the direction of the geomagnetic field. Since that field has a strong downwards component, the top of the pile resembles a magnetic south pole, i.e. a region in space where magnetic field lines appear to converge to. These two observations indicate that the geometry of the pile and the presence of the geomagnetic field create a distinct pattern in the magnetic stray field which might enable one to track the penetration from stray field measurements alone.

3 MODELLING OF THE STRAY FIELD

In this section, the magnetic signature of the pile is simulated to investigate whether the measured data can be captured by a simple model, which would serve as a basis to infer the current penetration depth of the pile from measured magnetic stray field data. To this end, an expression of the magnetic field at an evaluation point $\boldsymbol{B}(\boldsymbol{p})$ generated by the structure's magnetisation $\boldsymbol{M}(\boldsymbol{r})$ is derived, in which $\boldsymbol{r}$ represents all points within the volume of the pile. By applying the same expression to the internal points of the structure in conjunction with a suitable magnetic constitutive equation, the magnetisation induced by the external field is determined. Subsequently, the measured magnetic stray field is reproduced with a proposed simple expression for the magnetic susceptibility.

3.1 The stray field in the presence of an external field

Even though the external field is time and space invariant, the magnetisation of the pile will not be uniform due to the geometry of the structure, which leads to a significant demagnetising field [9]. To compute the magnetic field generated by the structure's magnetisation, a numerical approach applicable to steel sheets is adopted [10], which assumes that the magnetisation component in the normal direction of the sheet (the radial component M_r in the current situation) is negligible.

By evenly subdividing the pile's volume into N_θ elements in the circumferential and N_z elements in the axial direction, the structure is discretised, and the total number of elements equals $N = N_\theta N_z$. Under the assumption that the magnetisation is constant over each element and is concentrated at the element's barycentre $\boldsymbol{r}_i$, i.e. $\boldsymbol{M}(\boldsymbol{r}_i)$, the magnetic field at $\boldsymbol{p}$ is given

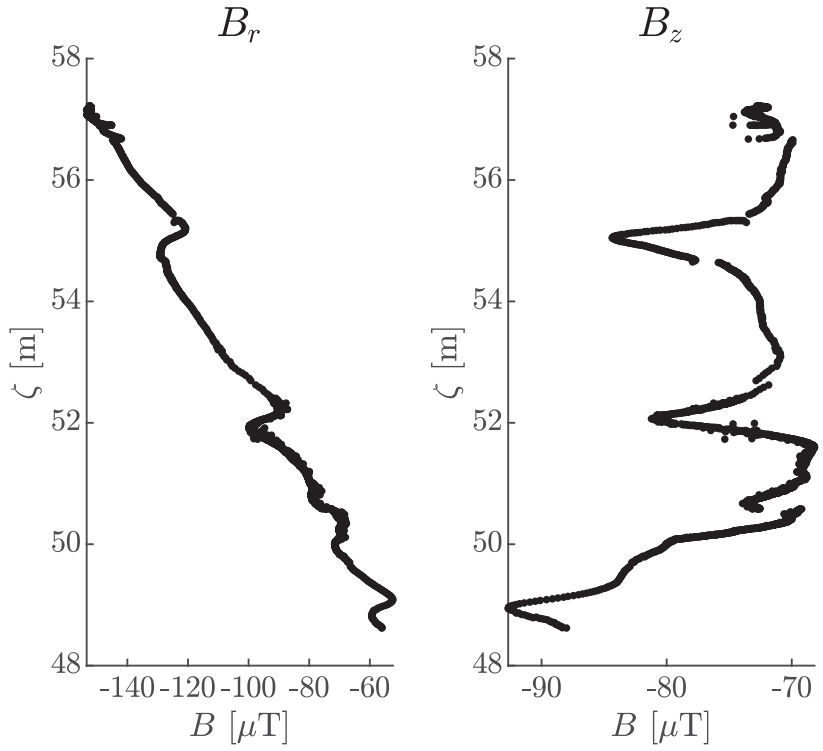

Figure 2: Remanent magnetic stray field versus the penetration depth.

by a summation of the contributions from all elements:

$$\boldsymbol{B}(\boldsymbol{p}) = \frac{\mu_0}{4\pi} \sum_{i=1}^{N} \oint_{\Gamma_i} \boldsymbol{M}(\boldsymbol{r}_i) \cdot \boldsymbol{n}_i \frac{\boldsymbol{p} - \boldsymbol{r}_i}{\|\boldsymbol{p} - \boldsymbol{r}_i\|^3} \, \mathrm{d}\Gamma_i, \tag{1}$$

in which μ_0 denotes the magnetic constant, and $\boldsymbol{n}_i$ is the outward normal to the element's boundary Γ_i. By evaluating the integrals, the expression above is rewritten:

$$\boldsymbol{B}(\boldsymbol{p}) = \mu_0 \sum_{i=1}^{N} \mathbf{G}_i \boldsymbol{M}(\boldsymbol{r}_i) = \mu_0 \mathbf{G}_{\boldsymbol{p}} \boldsymbol{M}, \tag{2}$$

in which $\mathbf{G}_i$ contains the values of the evaluated integrals for each element. In the latter part of the expression, these contributions are condensed into a single matrix $\mathbf{G}_{\boldsymbol{p}}$, and $\boldsymbol{M}$ is a vector incorporating the magnetisation components from all elements. Since the radial magnetisation component is deemed insignificant, $\boldsymbol{M}$ contains $2N$ entries.

To express the magnetisation in terms of the prevailing magnetic field, an appropriate constitutive equation is required. For a (locally) isotropic material, a scalar magnetic susceptibility χ suffices. Hence, the following implicit constitutive equation is employed:

$$\boldsymbol{M} = \chi \left(\frac{\boldsymbol{B}_0}{\mu_0} + \mathbf{G}_{\boldsymbol{r}} \boldsymbol{M} \right), \tag{3}$$

in which $\mathbf{G}_{\boldsymbol{r}}$ is a $2N \times 2N$ matrix representing the non-local interaction of the structure's magnetisation, which is obtained by substituting $\boldsymbol{r}_i$ for each element in Equation (2). Assuming that χ is not a function of the magnetisation itself, rearrangement of the former relation yields

$$\boldsymbol{M} = \chi \left(\mathbf{I} - \chi \mathbf{G}_{\boldsymbol{r}} \right)^{-1} \frac{\boldsymbol{B}_0}{\mu_0}, \tag{4}$$

in which $\mathbf{I}$ is the $2N \times 2N$ identity matrix and $(\cdot)^{-1}$ denotes a matrix inversion. When the susceptibility in known, the structure's magnetisation is computed by means of Equation (4); subsequently, the stray field at $\boldsymbol{p}$ is determined by employing Equation (2).

3.2 Model for the magnetic susceptibility

The experimental stray field data implies that the magnetic properties differ in the vicinity of the circumferential welds. Therefore, the following axial distribution of the magnetic susceptibility is proposed:

$$\chi = \chi_0 - \chi_w \left(\sin\left(\frac{\pi \left(z - z_0 \right))}{b} \right) \right)^n , \tag{5}$$

where χ_0 is the undisturbed susceptibility of the material, χ_w is the reduction of the susceptibility due to the presence of the weld, b is the distance between each weld, z_0 is an offset to correctly position the welds along the pile axis, and n is an even power to localise the reduced susceptibility to a narrow range around the weld's position. In this expression, b and z_0 are determined by the geometry of the pile alone, see Table 1. The numerical values of the remaining parameters have to be calibrated.

3.3 Simulated magnetic signature

To simulate the relative motion between the sensor and the pile, the stray field is evaluated along a line parallel to the axis of the pile, on which the evaluation points $\boldsymbol{p}$ are given in cylindrical $r\theta z$-coordinates by:

$$\boldsymbol{p} = \begin{bmatrix} R + d_m \\ \theta_m \\ \zeta + a_m - L \end{bmatrix} , \tag{6}$$

where $\zeta = [\zeta_0, \zeta_0 + 8.6]\,\mathrm{m}$, which coincides with the recorded penetration range. For these parameters, the corresponding numerical values are presented in Table 1. The volume of pile is discretised in $N_\theta = 25$ and $N_z = 300$ elements. In this case, the penetration is measured independently, and the unknown parameters in the susceptibility can easily be calibrated to match the measured results: $\chi_0 = 2100$, $\chi_w = 1600$, and $n = 20$. Figure 3a shows the susceptibility distribution resulting from these values.

The two components of the simulated magnetic field are presented in Figure 3b along side the measured data. Please note that the modelled values are shifted with a constant to match the measured signal; this shift represents the exact background field at the sensor location. From the figure, it is clear that the trend in the measured data is captured correctly by the simulated data. Only B_z differs for lower values of ζ, which might be attributed to other material inhomogeneities affecting the susceptibility which are not accounted for in the present model. Nonetheless, the simple relation for the magnetic susceptibility that accounts for the presence of circumferential welds is able to reproduce the measured magnetic signature of the pile.

4 DISCUSSION

The correspondence between the simulated magnetic signature and the measurements indicates that the simple susceptibility formulation given in Equation (5) is sufficient to model the magnetic state of the pile after a proper calibration is applied. In this case, the penetration depth is measured, significantly simplifying the calibration, since a fixed reference is present. Normally, however, this reference measurement of the penetration is obviously not available;

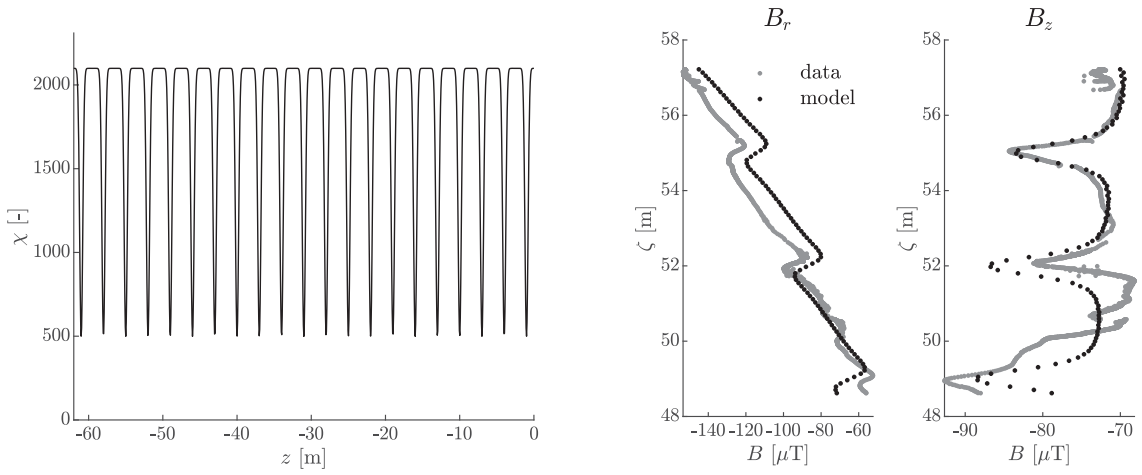

Figure 3: Model results for the magnetic stray field. (a) Modelled magnetic susceptibility along the pile's axis. (b) Modelled magnetic stray field versus the pile penetration compared to the measured data.

only the initial penetration depth is known to some extend. Therefore, the calibration should be founded solely on the measured magnetic field data. Fortunately, the welds create a distinct marking when they pass the sensor, e.g. a peak in the B_z value. Accordingly, as the weld positions are known at the start of the installation, the model can be calibrated based on the passage of one of those fixed markings, perhaps even constantly updating the model while new data is collected.

Once the model is calibrated, the penetration depth can be inferred by comparing the measured stray field to the modelled one. However, the mapping between some values of $\boldsymbol{B}$ and ζ is not unique (Figure 3b). Fortunately, the pile penetrates gradually into the soil; therefore, the penetration depth closest to the previous value should be selected. This additional step to extract the penetration depth from the magnetic data has not been elaborated yet, and it is left for future research.

The proposed method to monitor the pile's penetration has two benefits compared to currently used monitoring techniques; it relies on non-contact measurements, and it does not require an artificial tracking pattern applied to the pile's surface. In its current state, it only considers the magnetic stray field while the pile is unstressed. During the propagation of stress waves in the pile, reversible strain-induced magnetisation changes occur in conjunction to the changes related to the relative motion between the sensor and the pile, complicating the analysis considerably. Thus, the main application of the offered method is to monitor pile penetration during a full installation and not during a single hammer blow, e.g. a restrike test.

5 CONCLUSIONS

Based on magnetic stray field data collected during an onshore pile installation campaign, this paper proposes a new method to monitor the penetration of a steel monopile into the soil during pile driving. Contrary to state-of-the-art techniques, the proposed method is non-contact and does not require the introduction of an artificial pattern onto the surface of the structure. The latter is achieved by taking advantage of the naturally occurring pattern in the magnetic stray field as a result of circumferential welds in the pile. Furthermore, it is shown that this magnetic signature can be simulated by applying simple model for the magnetic susceptibility

proposed in this work. This modelled magnetic signature provides the basis for the method to monitor the penetration of a monopile during installation in real-time.

ACKNOWLEDGEMENTS

This research is part of the EUROS programme, which is supported by NWO domain Applied and Engineering Sciences and partly funded by the Dutch Ministry of Economic Affairs. The authors thank IHC-IQIP for the unique opportunity to perform these measurements at their yard in Sliedrecht, the Netherlands. Furthermore, the technical support provided by Arjan Roest (IHC-IQIP) and Kees van Beek (DEMO, TUDelft) is gratefully acknowledged.

REFERENCES

[1] P. Doherty and K. Gavin. "Laterally Loaded Monopile Design for Offshore Wind Farms". *Proceedings of the Institution of Civil Engineers - Energy* **165**.1 (2012), pp. 7–17. DOI: 10.1680/ener.11.00003.

[2] M. Schallert and O. Klingmüller. "Assessment of Soil Setup from Pile Installation Monitoring and Restrike Tests of Offshore Wind Turbine Foundation Piles". In: *10th International Conference on Stress Wave Theory and Testing Methods for Deep Foundations*. Ed. by P. Bullock, G. Verbeek, S. Paikowsky, and D. Tara. West Conshohocken, PA: ASTM International, 2019, pp. 681–696. DOI: 10.1520/STP161120170190.

[3] E. Wisotzki, R. van Foeken, P. van Esch, and D. Novakovic. "Strain and Acceleration Measurements at Instrumentation Distances to the Pile Head of 0.5 and 1.0 Times the Diameter—Offshore Pile-Monitoring Experience". In: *10th International Conference on Stress Wave Theory and Testing Methods for Deep Foundations*. Ed. by P. Bullock, G. Verbeek, S. Paikowsky, and D. Tara. West Conshohocken, PA: ASTM International, 2019, pp. 506–519. DOI: 10.1520/STP161120170238.

[4] S.-N. Lee, B.-J. You, M.-S. Limb, S.-R. Oh, S.-S. Han, and S. H. Lee. "Visual Measurement of Pile Penetration and Rebound Movement Using a High-Speed Line-Scan Camera". *Proceedings 2002 IEEE International Conference on Robotics and Automation (Cat. No.02CH37292)*. Vol. 4. 2002, 4307–4312 vol.4. DOI: 10.1109/ROBOT.2002.1014436.

[5] M.-S. Lim and J. Lim. "Visual Measurement of Pile Movements for the Foundation Work Using a High-Speed Line-Scan Camera". *Pattern Recognition* **41**.6 (2008), pp. 2025–2033. DOI: 10.1016/j.patcog.2007.10.025.

[6] J. R. M. S. Oliveira, P. R. R. L. Nunes, M. R. L. Silva, D. A. Cabral, A. C. G. Ferreira, L. A. V. Carneiro, and M. T. M. R. Giraldi. "Field Apparatus for Measurement of Elastic Rebound and Final Set for Driven Pile Capacity Estimation". *Geotechnical Testing Journal* **34**.2 (2011), p. 103103. DOI: 10.1520/GTJ103103.

[7] Y. Yeu, Y. S. Kim, and D. Kim. "Development of Safe and Reliable Real-Time Remote Pile Penetration and Rebound Measurement System Using Close-Range Photogrammetry". *International Journal of Civil Engineering* **14**.7 (2016), pp. 439–450. DOI: 10.1007/s40999-016-0053-y.

[8] A. Raza, U. Aqil, U. Baneen, and M. Q. Saleem. "Deep Foundation Testing Using Immunity-Based Displacement Measurement in Successive-Sparse Images". *KSCE Jour-*

nal of Civil Engineering **23**.10 (2019), pp. 4212–4222. DOI: 10.1007/s12205-019-2297-y.

[9] M. Beleggia, D. Vokoun, and M. De Graef. "Demagnetization Factors for Cylindrical Shells and Related Shapes". *Journal of Magnetism and Magnetic Materials* **321**.9 (2009), pp. 1306–1315. DOI: 10.1016/j.jmmm.2008.11.046.

[10] O. Chadebec, J.-L. Coulomb, V. Leconte, J.-P. Bongiraud, and G. Cauffet. "Modeling of Static Magnetic Anomaly Created by Iron Plates". *IEEE Transactions on Magnetics* **36**.4 (2000), pp. 667–671. DOI: 10.1109/20.877537.